AIAA JOURNAL
Vol. 49, No. 8, August 2011

High-Speed Boundary-Layer Instability: Old Terminology and a New Framework

Alexander Fedorov*
Moscow Institute of Physics and Technology, 140180, Zhukovsky, Russia
and
Anatoli Tumin†
University of Arizona, Tucson, Arizona 85721

DOI: 10.2514/1.J050835

The discrete spectrum of disturbances in high-speed boundary layers is discussed with emphasis on singularities caused by synchronization of the normal modes. Numerical examples illustrate different spectral structures and jumps from one structure to another with small variations of basic flow parameters. It is shown that this singular behavior is due to branching of the dispersion curves in the synchronization region. Depending on the locations of the branch points, the spectrum contains an unstable mode or two. In connection with this, the terminology used for instability of high-speed boundary layers is clarified. It is emphasized that the spectrum branching may cause difficulties in stability analyses based on traditional linear stability theory and parabolized stability equations methods. Multiple-mode considerations and direct numerical simulations are needed to clarify this issue.

Nomenclature

c	=	phase velocity
i	=	$\sqrt{-1}$
F	=	frequency parameter, ω/R
M	=	Mach number at the upper boundary-layer edge
Pr	=	Prandtl number
R	=	Reynolds number, $\sqrt{U_e^* x^*/\nu_e^*}$
$T(y)$	=	temperature profile of the mean flow
T_0	=	stagnation temperature
t	=	time
$U(y)$	=	velocity profile of the mean flow
x	=	downstream coordinate along the surface
y	=	vertical distance from the surface
α	=	wave number
ν	=	kinematic viscosity
ω	=	angular frequency

Subscripts

ad	=	adiabatic wall
e	=	upper boundary-layer edge
i	=	imaginary part
r	=	real part
w	=	wall condition

I. Introduction

IN HYDRODYNAMIC stability analysis, the normal mode concept suggests considering simple wavelike solutions of the linearized Navier–Stokes equations in the form $q'(x, y, t) = q(y)\exp(i\alpha x - i\omega t)$, where $q(y)$ is a complex amplitude function. This form assumes that the mean flow is parallel or quasi-parallel; i.e., the mean flow velocity and temperature profiles are functions of y only. The underlying idea of the normal mode concept is that instead of solving a specific physical initial-boundary-value problem, we consider normal modes of the wave system, expecting that a solution of the initial-boundary-value problem for the partial differential equations (PDEs) can be presented as a sum of the normal modes. If there is an unstable mode, it is expected that this mode will be present in the solution of a specific physical problem (realized experimentally or solved numerically) and it can be dominant after sufficient amplification in space and/or time. Because the continuum medium has an infinite number of degrees of freedom, the disturbance field has a numerable discrete spectrum or a continuous spectrum, or a combination of both [1,2].

In general, we may consider the wave number, $\alpha = \alpha_r + i\alpha_i$, and frequency, $\omega = \omega_r + i\omega_i$, as complex quantities. Very often two formulations are mentioned: temporal and spatial theories. In the temporal stability theory, $\alpha_i = 0$ and α_r is considered as a parameter, while ω is the complex frequency determined from the dispersion relation $\omega = \omega(\alpha, R, M, \ldots)$. According to the normal mode treatment, the solution depends on time as $\exp(-i\omega t) = \exp(-i\omega_r t + \omega_i t)$. It is unstable (grows exponentially with t) if $\omega_i > 0$, stable if $\omega_i < 0$, and neutral if $\omega_i = 0$. In the spatial stability theory, $\omega_i = 0$ and ω_r is the real frequency considered as a parameter, while the complex wave number α is determined from the dispersion relation $\alpha = \alpha(\omega, R, M, \ldots)$. Now the disturbance amplitude depends on the streamwise coordinate as $\exp(i\alpha x) = \exp(i\alpha_r x - \alpha_i x)$. Propagating downstream, the disturbance grows exponentially with x if $\alpha_i < 0$ and decays if $\alpha_i > 0$.

One can find in the literature an ambiguity with the choice between temporal or spatial formulations of stability problems. The ambiguity has its origin at the step when partial solutions of PDE are suggested in the form of normal modes. At this point, the link with the initial-boundary-value problem for a specific setup is lost, and we have an artificial dilemma of spatial-vs-temporal formulations.

Gustavsson [3] solved an initial-value problem for perturbations in the incompressible boundary layer. Salwen and Grosch [4] proved that Gustavsson's [3] solution is an expansion into the modes of discrete and continuous spectra of the temporal stability problem. The difference between the discrete spectrum and the continuous spectrum is their behavior outside the boundary layer ($y \to \infty$). The discrete spectrum is required to vanish as $y \to \infty$, while the continuous part is only required to be bounded. Ashpis and Reshotko [5] considered the signaling problem when a periodic-in-time point source introduces perturbations through the wall starting at $t = 0$. They showed that the solution of this problem can be presented (after

Presented at the 40th Fluid Dynamics Conference and Exhibit, Chicago, IL, 28 June–1 2010; received 5 August 2010; revision received 22 January 2011; accepted for publication 24 March 2011.

*Associate Professor, Department of Aeromechanics and Flight Engineering. Senior Member AIAA.

†Professor, Department of Aerospace and Mechanical Engineering. Associate Fellow AIAA.

a sufficiently long time when the transient effect is smeared out) as an expansion into modes of the discrete and continuous spectra resulted from the spatial stability theory. Therefore, the analysis of a specific initial-boundary-value problem for PDE leads to the unique expansion of a solution into the normal modes without any ambiguity. In compressible boundary layers, there are seven branches of continuous spectrum [6,7]: three branches correspond to waves propagating upstream with rapid decay, two branches correspond to slow and fast acoustic waves propagating downstream, and two branches correspond to vorticity and entropy waves propagating downstream.

Mack [8] discovered new unstable modes of the discrete spectrum in high-speed boundary layers. He first considered the temporal stability problem for inviscid perturbations and computed the eigenvalue dependencies $\omega(\alpha)$ for the flat plate boundary layer at various freestream parameters. In discussion of these dependencies, Mack used the terms modes and families. However, his usage of the term modes is inconsistent with the mathematical definition of modes as eigenfunctions that can be used for expansion of PDE solutions. Mack's definition of families is what mathematicians would normally call modes. Moreover, Mack subdivided a family representing one dependency of $\omega(\alpha)$ into different pieces giving them different labels of modes. To illustrate Mack's terminology, we refer to Fig. 1 showing the phase speed diagram $c_i(\alpha) = \omega_i(\alpha)/\alpha$ for the boundary layer on a thermally insulated (adiabatic) flat plate at the Mach number $M = 3.8$. One may compare Fig. 1 with Fig. 11.6a of [8]. Note that because we conduct computations at constant Prandtl number, $Pr = 0.72$, and in some cases at different stagnation temperature, there are some differences between our results and the results of [8]. Hereafter, dimensionless parameters are obtained using the Blasius length scale $\sqrt{\nu_e^* x^*/U_e^*}$ (asterisk denotes a dimensional quantity). Following Mack's notation, the wave numbers α_{sn} $(n = 1, 2, \ldots)$ are associated with the generalized inflection point at which $\mathrm{d}((\mathrm{d}U/\mathrm{d}y)/T)/\mathrm{d}y = 0$, and the wave numbers α_{1n} $(n = 1, 2, \ldots)$ are associated with regular neutral solutions.

Mack wrote ([8], pages 11–21),

> The eigenvalues for $c_i \neq 0$ lie on two separate curves in Fig. 11.6 and form distinct families of solutions. One family starts at the neutral sonic solution; the other starts at the first-mode regular neutral solutions. It is easier to discuss the inviscid solutions in terms of these families rather than in terms of the modes. The mode identification changes along the eigenvalue curves and is often not well defined.

Further down the same page, Mack introduces his definitions:

> In Fig. 11.6 the solutions of the c_0 family between $(0, c_0)$ and (α_{s1}, c_s) are amplified, and there is almost no phase change across the boundary layer in the pressure fluctuations. These solutions will be called first-mode amplified solutions. The solutions of the α_{11} family between $(\alpha_{11}, 1)$ and (α_{s2}, c_s) are also amplified, but except near $(\alpha_{11}, 1)$ there is a sizable phase change in the pressure fluctuations. These solutions will be called second-mode amplified solutions.

In the next paragraph on the same page, Mack introduces a definition of the other part of the c_0 family:

> It is of interest that there is a local maximum in the damping rate of the c_0 family of solutions at almost the same wave number for which the amplification rate of the solution of the α_{11} family is a maximum. Since the pressure-fluctuation phase change is large for the damped solutions near this wave number, those solutions will be called second-mode damped solutions.

Thus, Mack uses two different mode labels for one family curve.

The spectrum structure becomes more complicated at higher Mach numbers. For example, Fig. 2 shows $c_i(\alpha)$ at $M = 7$ (it is similar to Fig. 11.8a of [8]). In connection with this, Mack wrote on page 11–23 of [8],

> As shown in Fig. 11.8a for $M = 7$, the c_0 family of solutions no longer contains the first-mode neutral subsonic solution (α_{s1}, c_s) and the second-mode damped solutions, but instead contains the second-mode amplified solutions, the second-mode neutral subsonic solution (α_{s2}, c_s), and the third-mode damped solutions.

These examples illustrate that Mack's definitions of modes are inconsistent with conventional usage of the term normal modes. In Figs. 1 and 2, two distinct normal modes correspond to the c_0 and $(\alpha_{11}, 1)$ families.

Mack [8] then considered viscous perturbations and compared the dependencies of $c(\alpha)$ at finite Reynolds numbers with the inviscid ones. For one of Mack's choices of parameters, there were two "separate. . .inviscid amplification rate curves for the first and second modes" ([8], pages 12–24) (i.e., two inviscid normal modes), but "only a single amplification rate curve at the finite Reynolds number shown" (i.e., one viscous normal mode). This example illustrates that the spectrum structure can be drastically changed by the viscous effects.

Receptivity studies in the 1980s–2000s, which are summarized in [9,10], indicated that excitation of instabilities predominantly occurs upstream from the unstable region. This motivated Fedorov and Khokhlov [11] to investigate the disturbance spectrum in the region located upstream from the lower neutral branch. The spatial stability analysis [11] of 2-D unstable modes in hypersonic flows revealed the following features (Fig. 3):

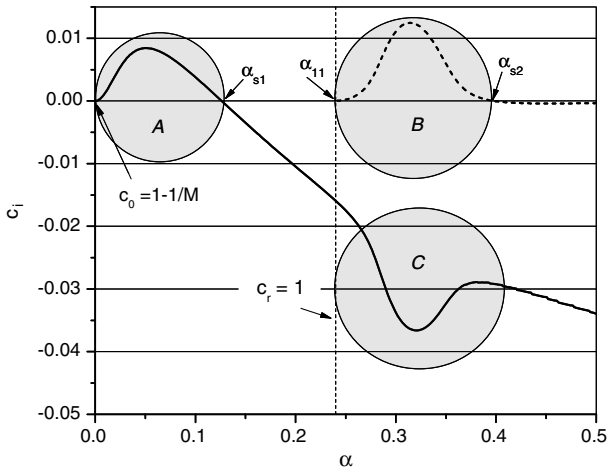

Fig. 1 Eigenvalue diagram at $M = 3.8$, $T_0 = 300$ K, $\gamma = 1.4$, and $Pr = 0.72$ with adiabatic wall and inviscid theory. Region A corresponds to first-mode amplified solutions. Region B corresponds to second-mode amplified solutions. Region C corresponds to second-mode damped solutions.

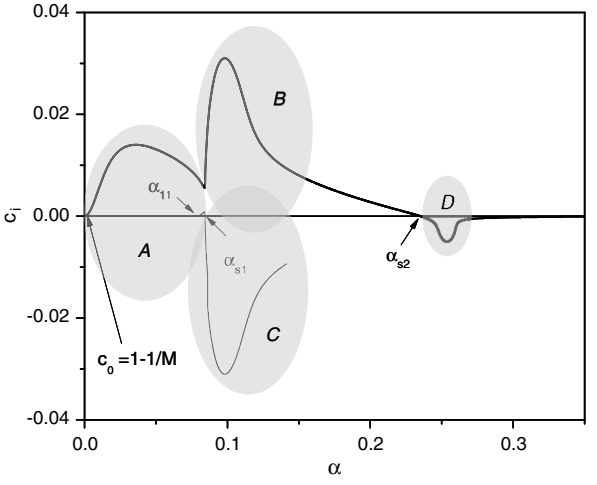

Fig. 2 Eigenvalue diagram at $M = 7$, $T_0 = 540$ K, $\gamma = 1.4$ $Pr = 0.72$, and $T_e = 50$ K with inviscid theory. Region A corresponds to first-mode amplified solutions. Region B corresponds to second-mode amplified solutions. Region C corresponds to second-mode damped solutions. Region D corresponds to third-mode damped solutions.

1) In the leading-edge region, two discrete modes (fast and slow) are synchronized with the fast and slow acoustic waves of the continuous spectrum, respectively.

2) Further downstream, the fast discrete mode is synchronized with the entropy and vorticity waves of the continuous spectrum.

3) Further downstream, the fast discrete mode is synchronized with the slow discrete mode. The latter synchronization leads to a branching of the discrete spectrum [12,13].

As shown in [11], the normal mode decomposition is not valid in the branch-point vicinity and should be replaced by a local solution accounting for the coupling of discrete modes. The consequences of these findings for modeling of high-speed transition are recently discussed by Fedorov [14].

The aforementioned shortcomings of Mack's terminology motivated Fedorov [9] to categorize the discrete modes using their asymptotic behavior near the leading edge. As shown in [11] for 2-D disturbances, the phase speed of one mode tends to $c = 1 - 1/M$ of slow acoustic wave, whereas the phase speed of the other tends to $c = 1 + 1/M$ of fast acoustic wave. Fedorov [9] called the former mode a slow mode (mode S) and the latter a fast mode (mode F). This terminology came to be used for the interpretation of direct numerical simulation results [15–18] on the receptivity and stability of high-speed boundary-layer flows.

The temporal stability analyses [19,20] revealed similar features of the spectral curves $\omega(\alpha)$ at fixed Reynolds number R. Namely, the fast (or slow) mode is synchronized with the fast (or slow) acoustic wave in the long-wave limit $\alpha \to 0$. As α increases, the fast mode is synchronized with the entropy/vorticity waves, and then it is synchronized with the slow mode that leads to branching of the discrete spectrum. The branching causes instability of what is called the second mode (according to Mack's terminology). This similarity is not surprising because the spectrum behavior depends on the product $\alpha^*\delta$. The case of $\alpha^* =$ fixed and $\delta \to 0$ is treated as a leading-edge limit, while the case of $\delta =$ fixed and $\alpha^* \to 0$ is treated as a long-wave limit.

Mack [8] introduced the viscous and inviscid families of solutions when the receptivity problem was not understood, and the decomposition of the solutions of the linearized Navier–Stokes equations had not been developed. A loose usage of the fist mode and the second mode terminology has not been an obstacle in discussion of linear stability theory applications to transition prediction (e.g., using the e^N method) even in the cases when only one unstable normal mode exists at finite Reynolds numbers. However, one has to be aware of the meaning of this imprecise terminology when transition prediction is based on consideration of the first and/or second mode. On the other hand, the usage of the mode F and mode S terminology has not yet been discussed properly in connection with the inviscid stability theory. In this paper, we consider the discrete spectrum of disturbances in high-speed boundary layers in order to clarify the contemporary terminologies and their interrelations. In addition, a model of discrete spectrum branching is outlined in order to explain different behaviors of the aforementioned discrete modes.

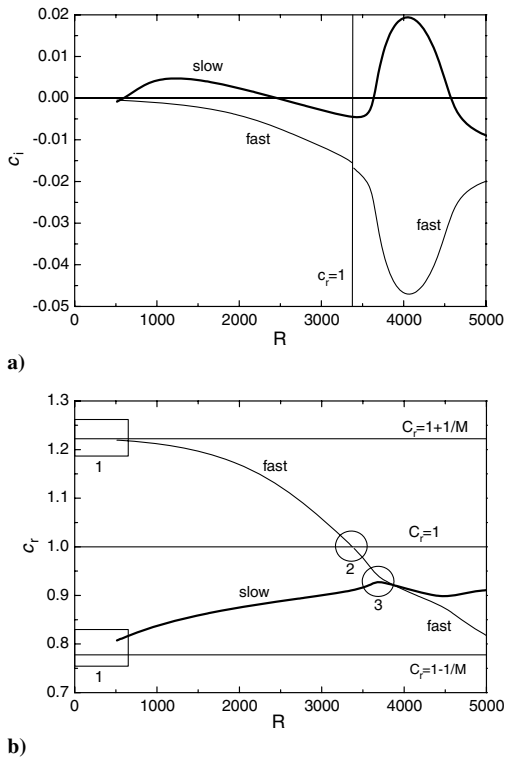

Fig. 3 Plots of a) imaginary and b) real parts of the phase speeds for slow and fast modes at $M = 4.5$, $T_w = T_{ad}$, and $F = 5 \times 10^{-5}$ with spatial stability analysis.

II. Discussion of Discrete Spectrum in High-Speed Boundary Layers

This section illustrates examples of discrete normal modes resulted from numerical solutions of the temporal and spatial stability problems for the locally parallel boundary-layer flow on a flat plate. All computations were conducted for perfect gas of constant Prandtl number $Pr = 0.72$ and specific heat ratio $\gamma = 1.4$. Viscosity is calculated using the Sutherland law with a constant of 110.4 K and the bulk viscosity is zero. The mean flow profiles correspond to the compressible Blasius solution; i.e., the viscos-inviscid interaction is neglected. The discrete spectrum structures for viscous (at finite Reynolds number) and inviscid ($R \to \infty$) disturbances are compared.

A. Temporal Stability Theory

To show the link between discrete modes at finite and infinite Reynolds numbers, we have to consider the regular neutral modes. The inviscid stability equations have neutral ($c_i = 0$) discrete solutions with the phase speed $1 \le c_r \le 1 + 1/M$. Figures 4a and 4b illustrate $c_i(\alpha)$ and $c_r(\alpha)$ for the boundary layer on an adiabatic flat plate at $M = 3.8$ and $R \to \infty$, and Figs. 5a and 5b show $c_i(\alpha)$ and $c_r(\alpha)$ at finite $R = 2000$. In the viscous case, the fast discrete mode, which is synchronized with fast acoustic wave of $c = 1 + 1/M$ as $\alpha \to 0$, has a small jump of $c_i(\alpha)$ at the point where $c_r = 1$. Actually, we should treat the fast mode as two discrete modes. One of them has $c_r > 1$ and coalescences with the continuous spectrum branch corresponding to vorticity and entropy waves ($c_r \to 1 + 0$). The other mode departs from this branch with $c_r \to 1 - 0$ and has $c_r < 1$. The coalescence and departure occur at slightly different values of c_i. Because the jump of c_i is small, it is usually ignored in stability analyses. However, the eigenfunctions are substantially different on different sides of $c_r = 1$. Their outer asymptotic forms contain different eigenvectors, which are proportional to $\exp(i\alpha x \pm i\lambda y - i\omega t)$ as $c_r \to 1 \mp 0$ and $y \to \infty$. This difference is important for analysis of the initial-value problem [19] describing receptivity to vorticity/entropy disturbances. Hereafter we call these modes as mode F_- and mode F_+. As shown in Fig. 5, mode F_- is associated with the regular neutral solutions in the inviscid limit. Mode S, which is synchronized with the slow acoustic wave of phase speed $c = 1 - 1/M$ as $\alpha \to 0$, corresponds to the inviscid slow mode shown in Figs. 4a and 4b. Mode F_+ is unstable at the range of relatively large α relevant to the second-mode instability. Mode S is unstable in the range of small α relevant to the first-mode instability.

Figures 6a and 6b illustrate $c_i(\alpha)$ and $c_r(\alpha)$ for the boundary layer on an adiabatic flat plate at $M = 4.2$ in the inviscid limit $R \to \infty$. The spectrum behavior is qualitatively the same as in the case of $M = 3.8$ (Figs. 4a and 4b). However, it is drastically different at the finite Reynolds number $R = 2000$ (Figs. 7a and 7b). Now there is only one unstable mode (mode S) that has two maxima of c_i associated with the two unstable regions. This is similar to Mack's observation in the cases of $M = 5.8$ and $M = 7$ ([8], page 12–24). Comparing the cases shown in Figs. 5a, 5b, 7a, and 7b we conclude that increasing of Mach number from 3.8 to 4.2 (at fixed $R = 2000$) leads to a qualitative change in the discrete spectrum pattern.

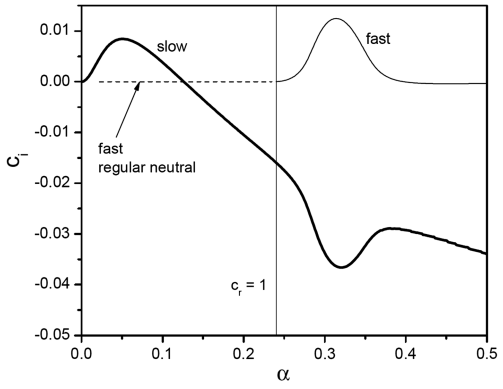

a)

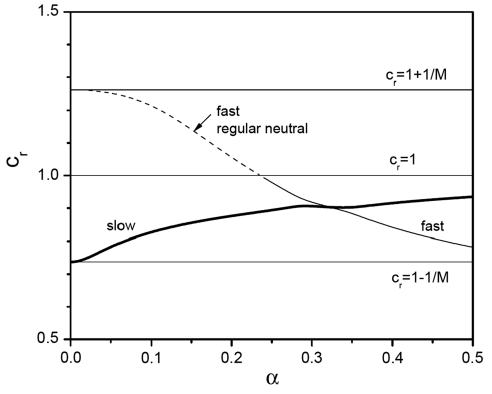

b)

Fig. 4 Plots of a) c_i and b) c_r versus α at $M = 3.8$ and $T_0 = 300$ K with inviscid theory.

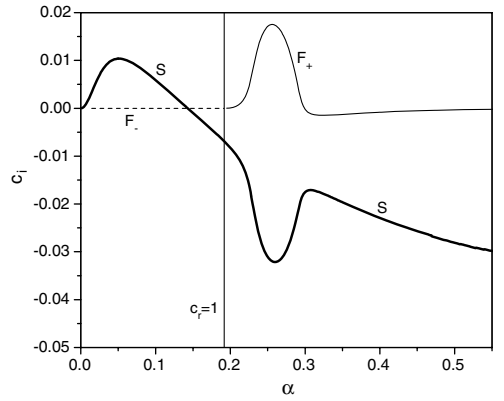

a)

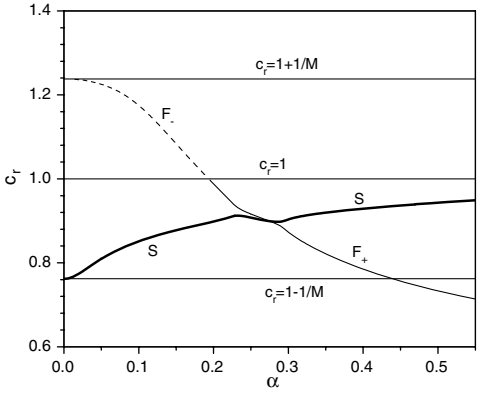

b)

Fig. 6 Plots of a) c_i and b) c_r versus α at $M = 4.2$ and $T_0 = 300$ K with inviscid theory.

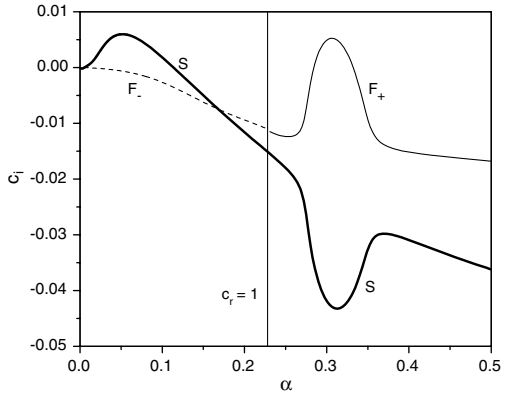

a)

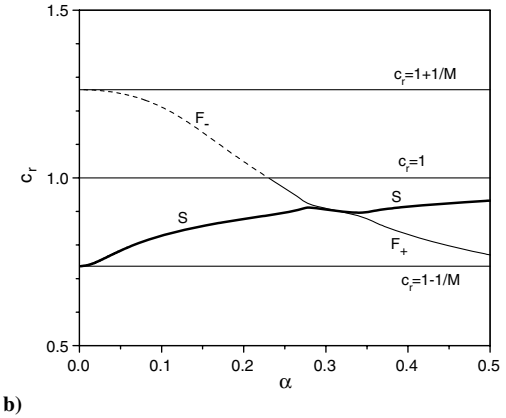

b)

Fig. 5 Plots of a) c_i and b) c_r versus α at $M = 3.8$, $T_0 = 300$ K, and $R = 2000$.

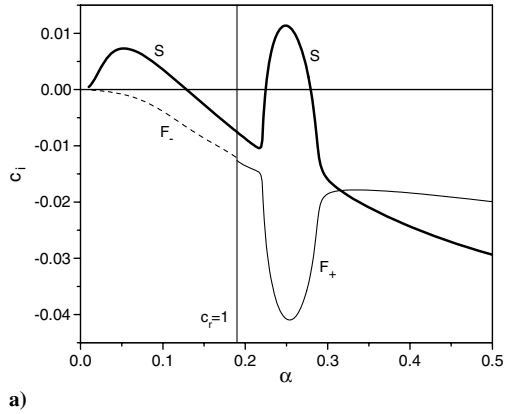

a)

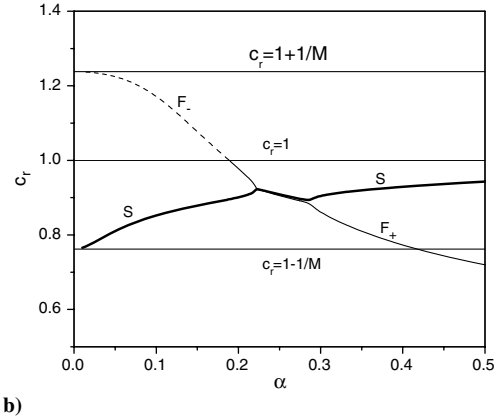

b)

Fig. 7 Plots of a) c_i and b) c_r versus α at $M = 4.2$, $T_0 = 300$ K, and $R = 2000$.

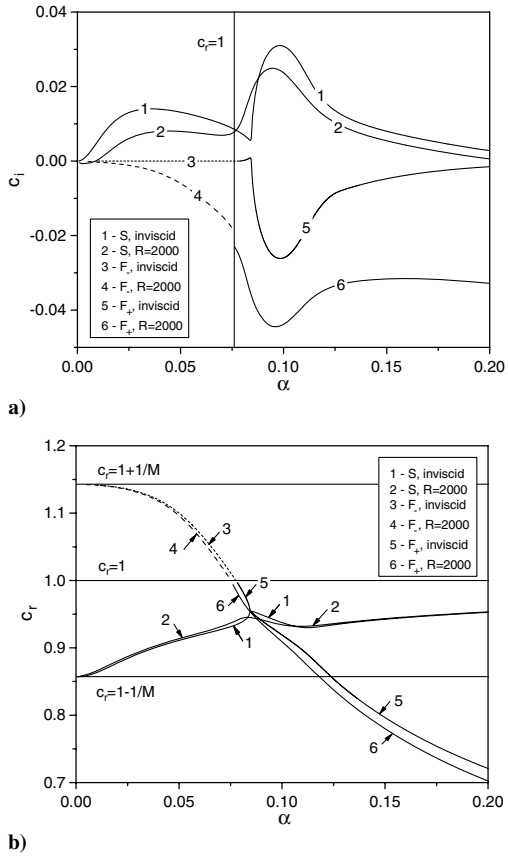

Fig. 8 Plots of a) c_i and b) c_r versus α in inviscid and viscous ($R = 2000$) analyses at $M = 7$ and $T_e = 50$ K.

Figures 8a and 8b shows c_i and c_r versus α for the inviscid and viscous cases at $M = 7$. Comparison of these data with that shown in Figs. 6a and 6b indicates that in the limit of $R \to \infty$ the discrete spectrum pattern switches over to a different topology somewhere in the range $4.2 < M < 7$. This change is similar to that observed for viscous disturbances in the Mach number range from 3.8 to 4.2.

B. Spatial Stability Theory

1. Adiabatic Wall

In the case of an adiabatic wall in the spatial theory, available numerical results indicate that there is only one unstable mode (mode S). Figures 9a and 9b show α_i versus frequency at $M = 3.8$ and fixed Reynolds numbers. One can see that there are two minima in $\alpha_i(\omega)$. At $R = 600$, only the first minimum represents spatially unstable solutions. At $R = 2000$, unstable perturbations can be found in two bands of frequencies. Plotting the neutral curves in the ω-R plane shows two unstable regions, but both of them are associated with mode S.

Another example is shown in Fig. 10 for the case of $M = 4.2$ and $R = 2000$. Again, mode S is unstable in the low-frequency band relevant to the first-mode instability and in the high-frequency band relevant to the second-mode instability.

2. Cold Wall

It was shown in [11] that mode F_+ can be unstable as well. To illustrate the spectral pattern, we consider perturbations at a fixed frequency parameter $F = \omega^* \nu_e^* / U_e^{*2}$. The dimensionless angular frequency is $\omega = F \times R$, the eigenvalues and phase speeds are expressed as $\alpha = \alpha(R)$, $c(R) = \omega/\alpha(R)$.

Figures 11 and 12 show $\alpha_i(R)$ and $c_r(R)$ of modes S, F_- and F_+ for the boundary-layer flow at $M = 5.5$ and $M = 6.5$, respectively. In both cases, the mean-flow temperature at the upper boundary-layer edge is $T_e^* = 70$ K, the wall temperature is $T_w = 0.1 T_{\text{ad}}$, and the frequency parameter is $F = 10^{-4}$. Similar to the temporal stability

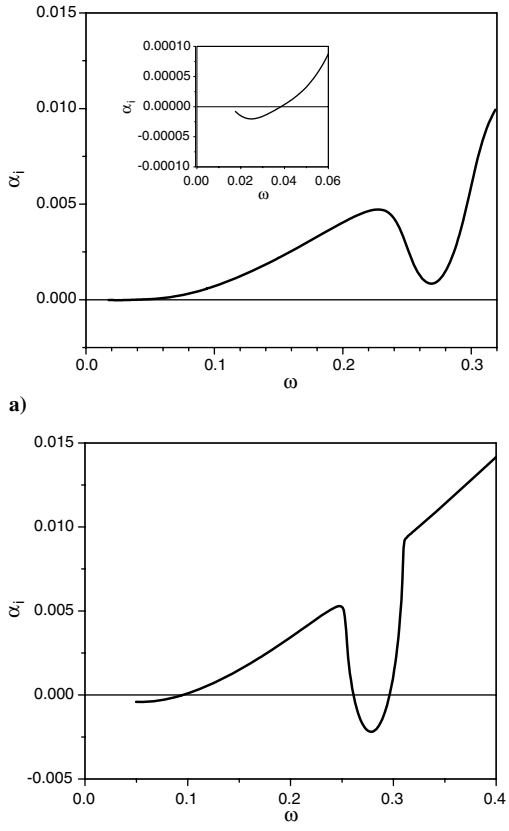

Fig. 9 Plots of α_i versus ω for mode S at a) $R = 600$ and b) $R = 2000$; $M = 3.8$ and adiabatic wall.

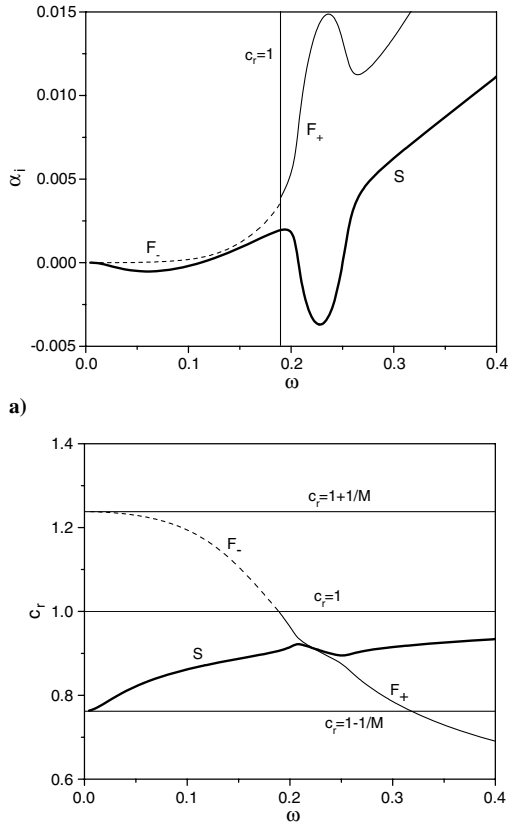

Fig. 10 Plots of a) α_i and b) c_r versus ω at $M = 4.2$, $T_0 = 300$ K, and $R = 2000$ with adiabatic wall.

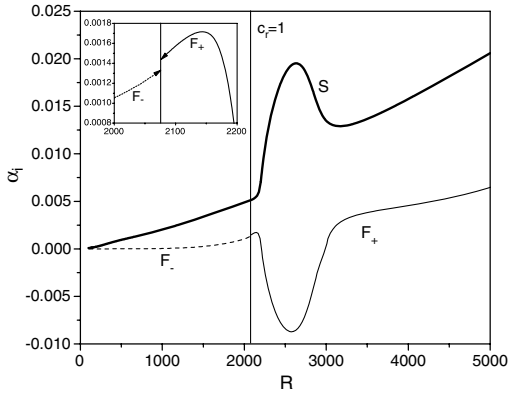

a)

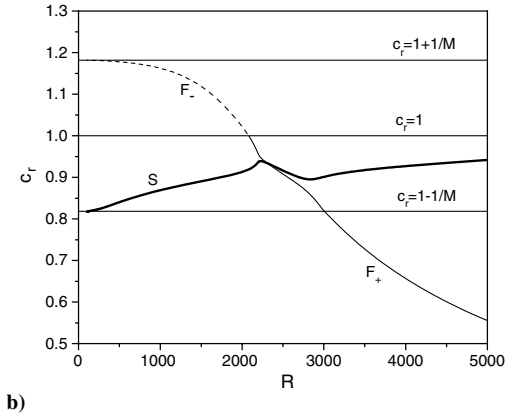

b)

Fig. 11 Plots of a) α_i and b) c_r versus R at $M = 5.5$, $T_e = 70$ K, $T_w/T_{ad} = 0.1$, and $F = 10^{-4}$.

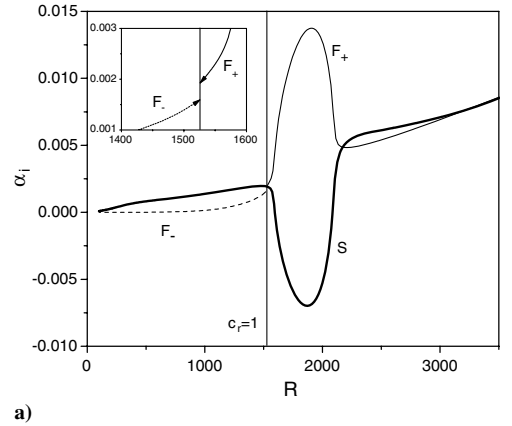

a)

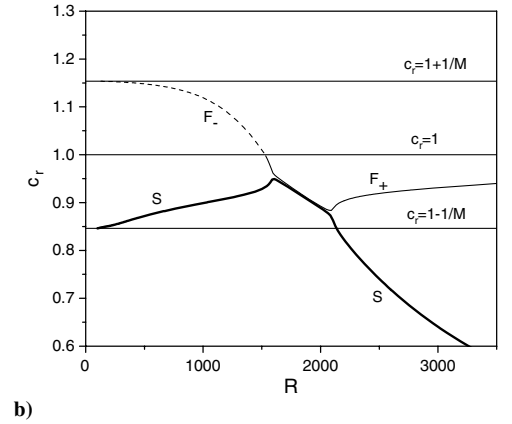

b)

Fig. 12 Plots of a) α_i and b) c_r versus R at $M = 6.5$, $T_e = 70$ K, $T_w/T_{ad} = 0.1$, and $F = 10^{-4}$.

cases discussed in Sec. II.A, mode F_- (or mode S) is synchronized with the fast (or slow) acoustic wave in the leading-edge region corresponding to the long-wave limit. Then mode F_- is synchronized with vorticity/entropy waves of the continuous spectrum at the station where $c_r = 1$. As the fast-mode eigenvalue crosses the vorticity/entropy branch, its imaginary part jumps by a small value $\Delta\alpha_i$. Further downstream mode F_+ is synchronized with mode S and the dispersion curves branch out.

In the case of $M = 5.5$ (Figs. 11a and 11b), the branching leads to destabilization of mode F_+ and stabilization of mode S in the range of R relevant to instability of Mack's second mode. As contrasted to the adiabatic wall cases, there is no instability of the slow mode at relatively small R because this instability (associated with Mack's first mode) is suppressed by the wall cooling. In the case of $M = 6.5$ (Figs. 12a and 12b), the branching is qualitatively different. Now mode S is unstable and mode F_+ is stable. Detailed computations showed that the switching from one topology to the other occurs at $M \approx 6$.

III. Model of the Discrete Spectrum Branching

Guschin and Fedorov [12,13] realized that the aforesaid branching of discrete spectrum is similar to the branching of weakly coupled waves that is typical for wave systems in the physics of plasmas [21] (see also Sec. 64 of [22]). Herein, we outline an analytical model describing this branching.

Consider the temporal spectrum $\omega(\alpha)$ and assume that the eigenvalues $\omega_1(\alpha)$ and $\omega_2(\alpha)$ (in our case, they are relevant to modes F_+ and S) are synchronized in the vicinity of a certain point α_0: $\omega_1(\alpha_0) \approx \omega_2(\alpha_0) \approx \omega_0$. The other modes of the discrete and continuous spectra are assumed to be sufficiently far from the synchronization region. Then the dispersion relation in the vicinity of (α_0, ω_0) can be approximated as

$$(\bar{\omega} - a_1\bar{\alpha})(\bar{\omega} - a_2\bar{\alpha}) = \varepsilon_t \tag{1}$$

where $\bar{\omega} = \omega - \omega_0$ and $\bar{\alpha} = \alpha - \alpha_0$ are local variables, ε_t is a small parameter characterizing weak coupling between the modes, and $a_1 > a_2 > 0$ are the group velocities of the decoupled modes (at

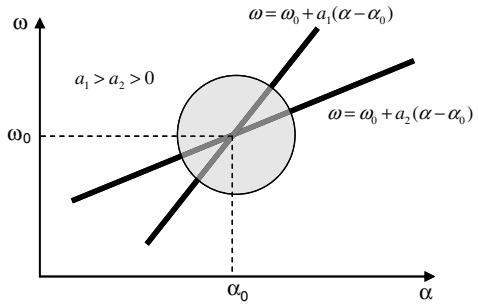

Fig. 13 Synchronization of two uncoupled modes in the vicinity of (α_0, ω_0).

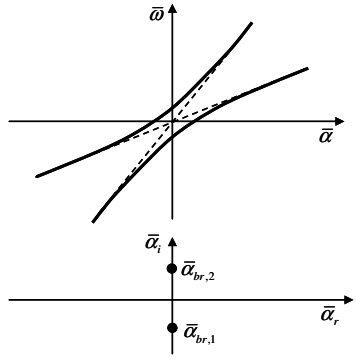

Fig. 14 Neutral branching at $\varepsilon_t > 0$.

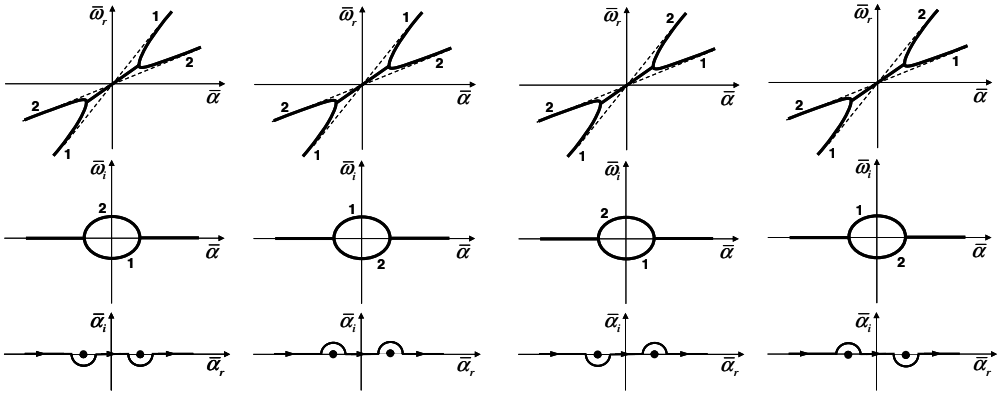

Fig. 15 Branching patterns for two weakly coupled modes.

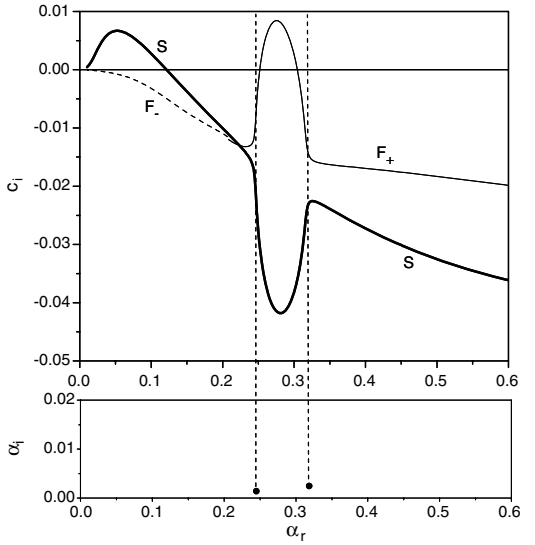

a)

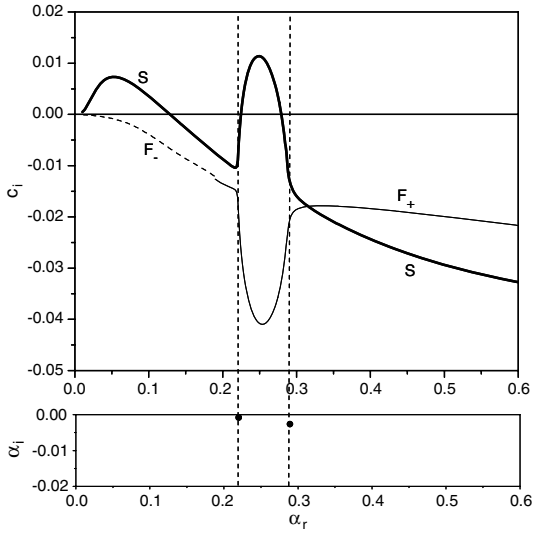

b)

Fig. 16 Different branching patterns at small variation of the Mach number at $T_0 = 300$ K and $R = 2000$. Branch points are shown by black circles in the complex α plane: a) $M = 4$, branch points are bypassed from below (branching A) and b) $M = 4.2$, branch points are bypassed from above (branching B).

$\varepsilon_t = 0$) schematically shown in Fig. 13. The dispersion curves branch out in the vicinity of the synchronization point as

$$\bar{\omega}_{1,2} = \frac{a_1 + a_2}{2}\bar{\alpha} \pm \sqrt{\frac{1}{4}\bar{\alpha}^2(a_1 - a_2)^2 + \varepsilon_t} \tag{2}$$

The branching pattern depends on the locations of the branch points $\bar{\alpha}_{\mathrm{br}1,2} = \mp 2\sqrt{-\varepsilon_t}/(a_1 - a_2)$ in the complex α plane. If $\varepsilon_t > 0$, then $\bar{\alpha}_{\mathrm{br}1,2}$ are pure imaginary and the dispersion curves branch out, as shown schematically in Fig. 14. In this case, the coupling does not cause instability. If $\varepsilon_t < 0$, the branch points are real and $\bar{\omega}_{1,2}$ are complex values in the range $\bar{\alpha}_{br1} < \bar{\alpha} < \bar{\alpha}_{br2}$. In this case, one mode becomes stable and the other unstable. Depending on bypasses of the branch points, there are four patterns of dispersion curves, as shown schematically in Fig. 15.

For the temporal spectra of the boundary-layer flow discussed in Sec. II.A, the branching of modes F_+ and S is topologically identical with one of the patterns shown in Fig. 15. The branch points were determined numerically from the condition $|\partial\omega/\partial\alpha|^{-1} = 0$. Computations showed that $\alpha_{\mathrm{br}1,2}$ are slightly shifted from the real axis to the lower or upper half-plane of complex α depending on the basic flow parameters. As one marches along real α, the branch points are bypassed from above or below, leading to a particular branching pattern.

The branch points move in the α plane with variations of the flow parameters, say the Mach number. As soon as α_{br} crosses the real axis, the branching pattern switches over from one to another. For example, Fig. 16 shows such switching from the branching A to the branching B, due to a slight increase of Mach number from 4 to 4.2.

By computing the trajectories of the branch points and determining the parameters at which $\alpha_{\mathrm{br}1,2}$ crosses the real axis one can identify domains relevant to different branching patterns. As an example, Fig. 17 shows the boundary between the branching A and the branching B in the Mach number-wall temperature plane. Below this boundary (at the relatively cold wall condition) there are two unstable modes: mode S is unstable in the range of small α and mode F_+ is unstable in the range of large α. Above this boundary, there is only one unstable mode—the slow mode.

Similar analysis can be conducted for the spatial stability problem [11]. The dispersion relation is analytically continued to the complex plane of R. In the vicinity of synchronization point (R_0, α_0), Eq. (1) is written in the form

$$(\bar{\alpha} - b_1\bar{\omega})(\bar{\alpha} - b_2\bar{\omega}) = \varepsilon_s \tag{3}$$

where $\bar{\alpha} = \alpha - \alpha_0$, $\bar{\omega} = F(R - R_0) = F\bar{R}$, $b_1 = a_2^{-1}$, and $b_2 = a_1^{-1}$ are constants ($b_1 > b_2 > 0$), and a small parameter $\varepsilon_s = \varepsilon_t/(a_1 a_2)$ characterizes the coupling between synchronized modes. The solution has two branches

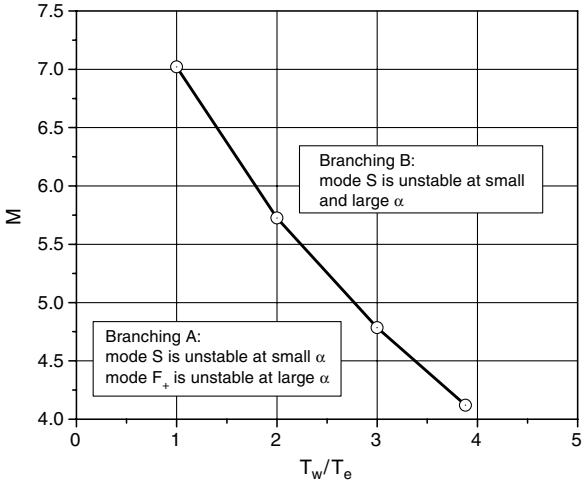

Fig. 17 Mach numbers and wall temperature ratios relevant to different branching patterns, $T_0 = 300$ K, $R = 2000$.

$$\bar{\alpha}_{1,2} = \frac{b_1 + b_2}{2} F\bar{R} \pm \sqrt{\frac{1}{4}(b_1 - b_2)^2 F^2 \bar{R}^2 + \varepsilon_s} \qquad (4)$$

The branch points $\bar{R}_{\mathrm{br}1,2} = \mp 2\sqrt{\varepsilon_s}/[F(b_1 - b_2)]$ are located in different half-planes of complex $\bar{R}$ depending on the basic flow parameters. With marching downstream along real R, the branch points are bypassed from above or below that leads to different branching patterns of $\alpha(R)$. For instance, in the case of $M = 5.5$ (Fig. 11), both branch points lie above the real axis of complex R plane that gives the branching A shown in Fig. 15. In the case of $M = 6.5$ (Fig. 12), the first branch point is below the real axis and the second is above. This gives the branching D.

Thus, the analytical model of weakly coupled synchronized modes helps to interpret intricate behaviors of disturbance spectrums that are observed in high-speed boundary layer flows. This model clearly shows that the second-mode instability is due to synchronization of modes S and F_+. Similar mechanism is responsible for the third- and higher-mode instabilities in hypersonic boundary layers [13], as well as short-wave instabilities in a thin shock layer [23]. As an example, Figs. 18 and 19 show the discrete spectrum at $M = 7$, $T_e = 50$ K and $R = 20000$ in the case of adiabatic wall ($T_w = T_{\mathrm{ad}}$) and cold wall ($T_w = 1.2T_e$), respectively. In both cases, there are fast modes $F_\pm^{(1)}$, $F_\pm^{(2)}, \ldots$ and the slow mode S. On an adiabatic wall, Mack's second, third, etc., instabilities correspond to mode S. These instabilities are associated with the branching B between modes $F_+^{(k)}$ and mode S. In the cold-wall case, Mack's second, third, etc., instabilities correspond to modes $F_+^{(1)}$, $F_+^{(2)}$, etc. These instabilities are associated with the branching A. As the number k of mode $F_+^{(k)}$ increases, the growth rates quickly decreases; e.g., the mode $F_+^{(3)}$ in Fig. 19a is almost neutral. Ma and Zhong [24,25] showed that the fast modes $F_-^{(1)}$, $F_-^{(2)}$, etc. (named modes I, II, etc., in [24]) are effectively excited by fast acoustic waves.

Fedorov and Khokhlov [11] showed that the normal mode decomposition is not valid near the branch point of discrete spectrum.

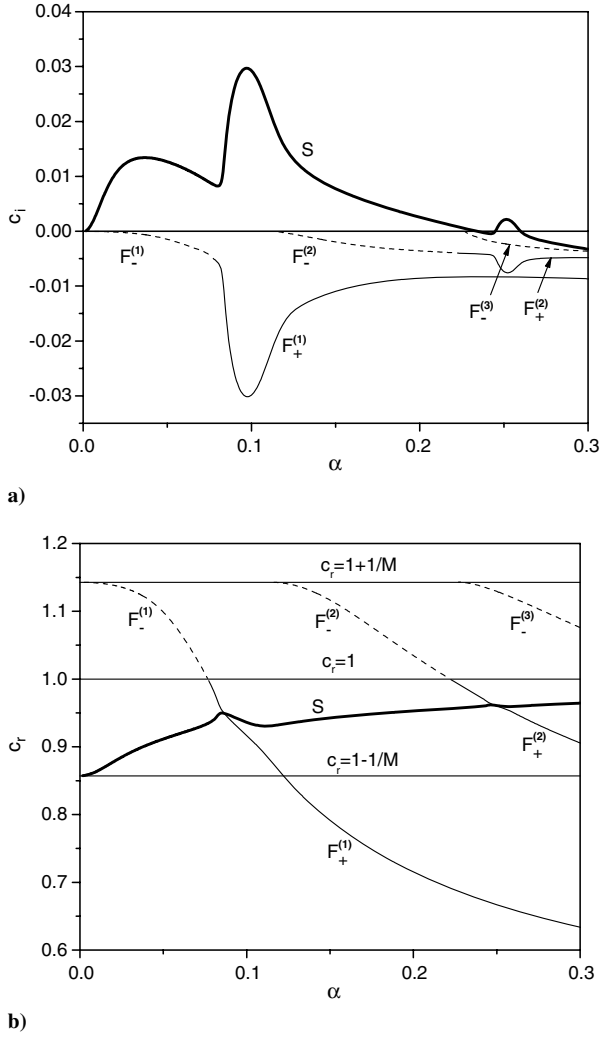

Fig. 18 Plots of a) c_i and b) c_r versus α at $M = 7, T_e = 50$ K, $R = 20000$ with an adiabatic wall.

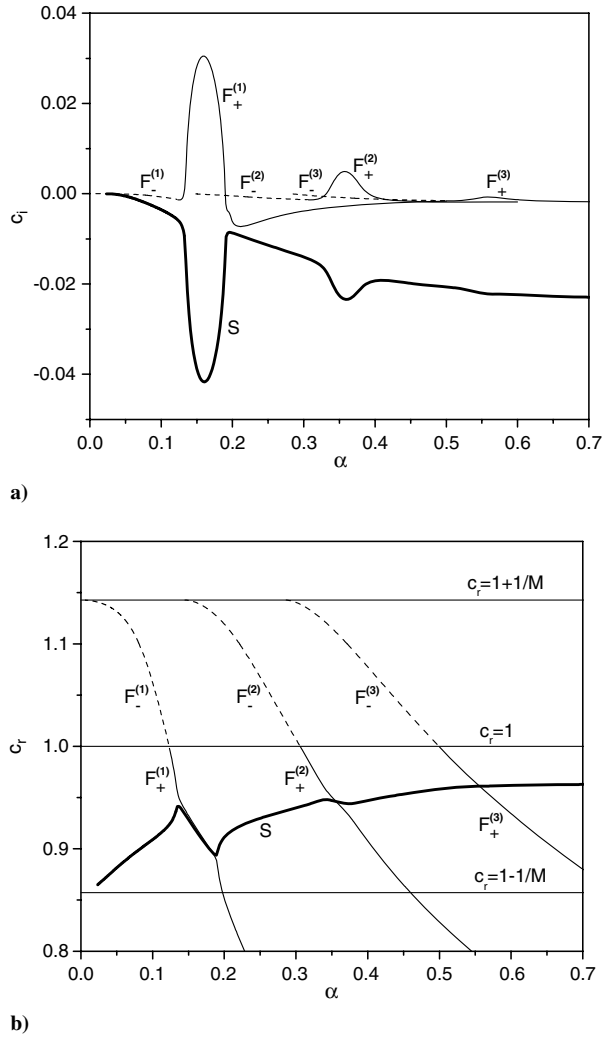

Fig. 19 Plots of a) c_i and b) c_r versus α at $M = 7$, $T_e = 50$ K, and $R = 20000$, with cold wall $T_w = 1.2T_e$.

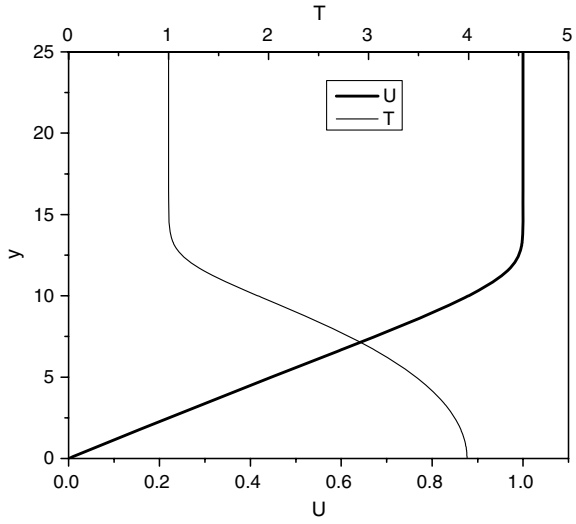

Fig. 20 Mean-flow profiles at $M = 4.2$, $T_0 = 300$ K, and $T_w = T_{ad}$.

Using asymptotic methods they obtained a local solution providing coupling between input and output amplitudes of the branching modes. It turned out that this coupling is governed by the intermodal exchange rule, which, in the leading-order approximation, does not depend on the mean-flow profiles. However, this result may be not valid when the branch point is too close to the branch cut of continuous spectrum; e.g., Fig. 16 shows that the relative distance between the first branch point $\alpha_{b1} = 0.2199 - i0.00075$ and the vorticity/entropy branch cut is $\Delta\alpha/\alpha \approx 5\%$. In this case the vorticity/entropy waves may significantly affect the intermodal exchange. This issue should be clarified by further theoretical studies.

IV. Eigenfunctions of Slow and Fast Modes

Now we consider the eigenfunctions of the slow and fast modes for the boundary-layer flow at $M = 4.2$, $R = 2000$ and $T_w = T_{ad}$ (see Figs. 7a and 7b). In all cases discussed herein, the eigenfunctions are normalized to the absolute value of the pressure amplitude on the wall. Perturbations of pressure p, streamwise velocity u and temperature θ are made nondimensional using $\rho_e^* U_e^{*2}$, U_e^* and T_e^*, respectively. Figure 20 shows the mean-flow profiles $U(y)$ and $T(y)$, where the boundary-layer thickness is $\delta = 12.5$ ($U(\delta) = 0.99$) and the displacement thickness is $\delta_1 = 9.34$.

At $\alpha = 0.05$ relevant to the first instability maximum, the eigenfunction of mode F_- typifies regular disturbances of the phase speed $c_r > 1$ (thin lines in Fig. 21). The slow mode (thick lines) of $c_r = 0.81$ has the critical layer in the vicinity of $y_c \approx 10$. Here the u-velocity distribution has a phase jump and the temperature amplitude $|\theta|$ has a strong maximum. The pressure amplitude $|p|$ is almost constant across the boundary layer as typical for long-wave disturbances. Near the wall ($0 < y < 1.2$) there is a well distinguished viscous sublayer (Stokes layer) for both fast and slow modes.

Figure 22 shows eigenfunctions of modes F_- and F_+, which are synchronized with the entropy and vorticity waves at $c_r \to 1 \pm 0$. These functions are almost identical inside the boundary layer, while the tails for the u velocity and temperature are essentially different outside the boundary layer. This clearly shows that mode F_- with $c_r > 1$ and mode F_+ with $c_r < 1$ are different normal modes of the

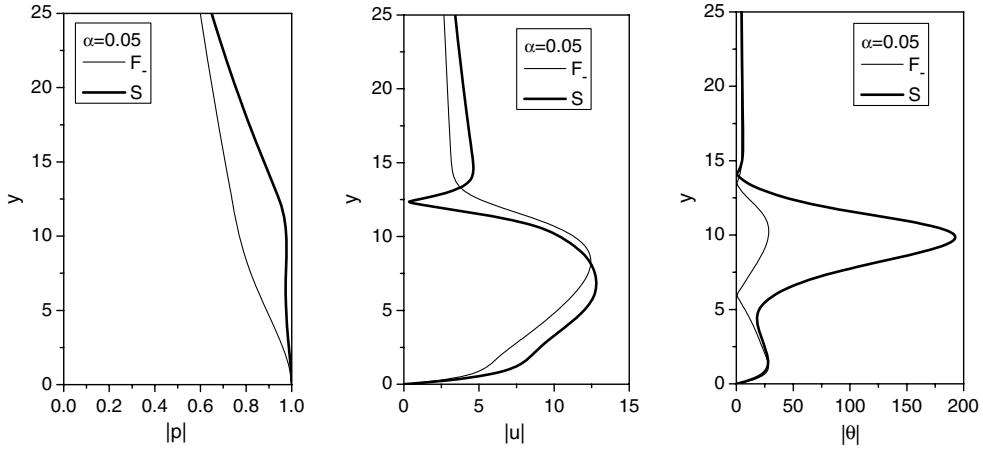

Fig. 21 Eigenfunctions of the fast and slow modes at $\alpha = 0.05$, $M = 4.2$, $T_0 = 300$ K, $T_w = T_{ad}$, and $R = 2000$.

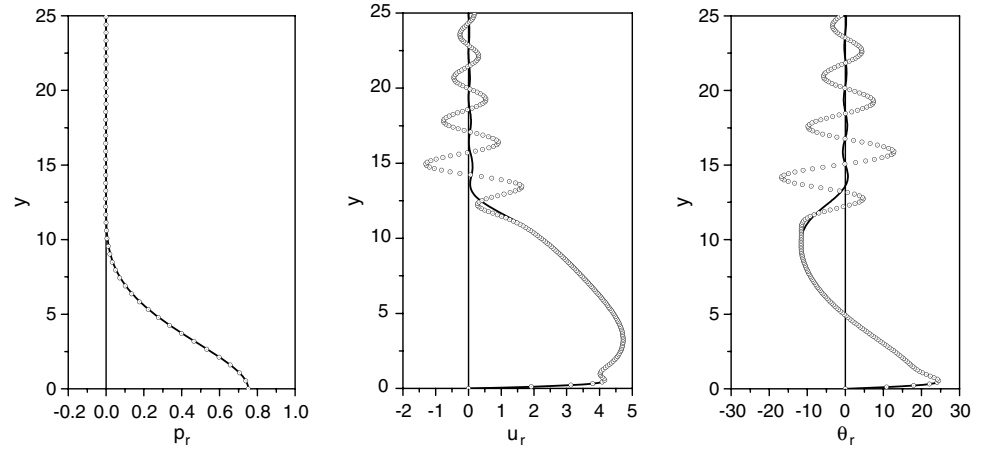

Fig. 22 Eigenfunctions of fast modes in the vicinity of vorticity and entropy waves at $M = 4.2$, $T_0 = 300$ K, $T_w = T_{ad}$, and $R = 2000$. Symbols indicate mode F_+ at $\alpha = 0.1899$ and $c_r \to 1 - 0$; black lines indicate mode F^- at $\alpha = 0.1886$ and $c_r \to 1 + 0$.

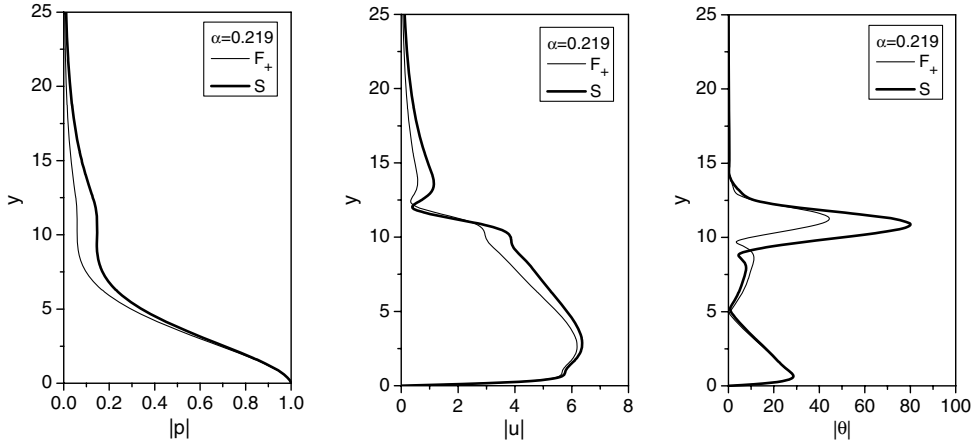

Fig. 23 Eigenfunctions of modes F_+ and S in the vicinity of the first branch point, $M = 4.2$, $T_0 = 300$ K, $T_w = T_{ad}$, $R = 2000$, and $\alpha = 0.219$.

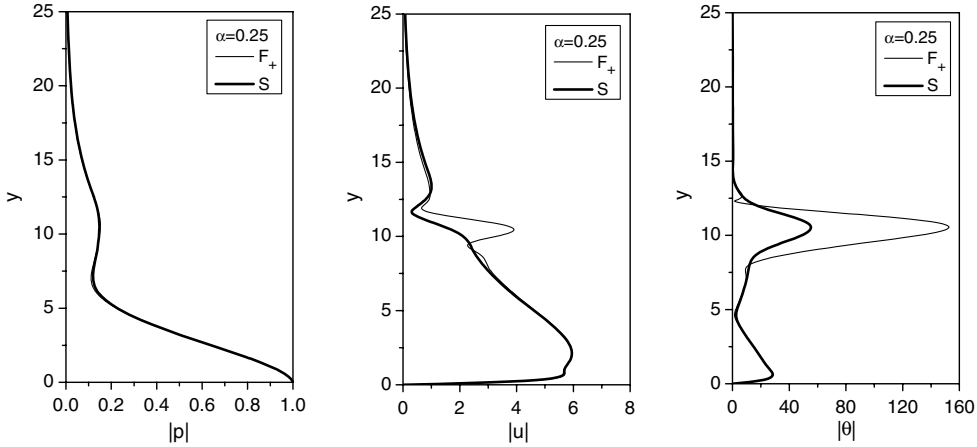

Fig. 24 Eigenfunctions of fast and slow modes at $\alpha = 0.25$, $M = 4.2$, $T_0 = 300$ K, $T_w = T_{ad}$, and $R = 2000$.

discrete spectrum. The oscillatory behavior of the outer tails is due to synchronization of the discrete modes with the entropy and vorticity waves, which oscillate in the outer flow. A detailed discussion of these spectrum features is given in [19].

Figure 23 shows eigenfunctions of modes S and F_+ in the vicinity of the first branch point $\alpha_{br1} = 0.2199 - i0.00075$ (see branching B in Fig. 16). As expected, in this region both modes have similar distributions across the boundary layer. However, there are quantitative differences because the eigenfunctions were computed at $\alpha = 0.219$ which is slightly shifted from the branch point.

Figure 24 illustrates eigenfunctions at $\alpha = 0.25$ relevant to the second maximum of instability (see Fig. 7a). This point lies approximately in the middle of the branching region $\alpha_{br1} < \alpha < \alpha_{br2}$, where the coupling between modes F_+ and S produces the most profound effect on the growth rates. Since the real frequencies of these modes are practically identical, their eigenfunctions are very close everywhere besides the critical layer, which is formed at the distance $y_c \approx 10$.

The foregoing examples show that the eigenfunctions of fast and slow modes are quite sensitive to singularities of the dispersion relation caused by spectrum branching and by coalescence with the continuous spectrum. This may significantly affect receptivity as well as the nonlinear interaction between the modes.

V. Conclusions

The structure of the discrete spectrum in stability analysis of high-speed boundary layers depends on basic flow parameters such as the Mach number, Prandtl number, Reynolds number, etc. The spectrum may have two unstable modes that are easily associated with inviscid instabilities of Mack's first and second modes. With another choice of the basic parameters, the spectrum may have only one unstable mode having two maxima of the growth rate.

Terminology using modes 1 and 2 (the well-known first and second modes) is inconsistent with a proper mathematical treatment of normal modes. Mack's family of solutions is actually what should be called a normal mode, whereas his definitions of first-mode amplified solutions and second-mode amplified/damped solutions lead to confusion when normal modes are used to represent a solution of the linearized Navier–Stokes equations. The advances of the last decades have made necessary to develop new terminology to replace the old. In mathematical analysis of the initial-value problems, it is more convenient to follow the terminology: fast (F) and slow (S) modes. According to this terminology discrete modes $F_-^{(k)}$ ($k = 1, 2, \ldots$) are synchronized with fast acoustic waves of the continuous spectrum at sufficiently small R in the spatial framework or at sufficiently small α in the temporal framework. These modes have $c_r > 1$ and correspond to the regular neutral solutions in the inviscid limit. The discrete mode S is synchronized with slow acoustic wave of the continuous spectrum as $R \to 0$ in the spatial framework or as $\alpha \to 0$ in the temporal framework. As R (or α) increases, the phase speed of $F_-^{(k)}$ decreases, and these modes are ultimately absorbed by the continuous spectrum of vorticity/entropy waves at $c_r = 1 + 0$. Simultaneously modes $F_+^{(k)}$ spring from the continuous spectrum at $c_r = 1 - 0$, with c_i being slightly different from c_i of corresponding modes $F_-^{(k)}$. Although the jump of c_i is very small and is usually ignored in stability computations, the eigenfunction of mode $F_-^{(k)}$ at $c_r = 1 + 0$ is essentially different from the eigenfunction of $F_+^{(k)}$ mode at $c_r = 1 - 0$. This difference should be taken into account in solving the initial-value problem associated with receptivity to vorticity/entropy waves.

Depending on the flow parameters, both mode S and modes $F_+^{(k)}$ can be unstable or only mode S is unstable having several maxima of the growth rate. The low-frequency (long-wavelength) maximum is associated with Mack's first mode, whereas the higher-frequency (shorter-wavelength) maxima are associated with Mack's second mode, third mode, etc. The second-mode instability is due to the branching of modes S and $F_+^{(1)}$ in the vicinity of their synchronization, the third-mode instability is due to the branching of modes S and $F_+^{(2)}$, etc. Because this mechanism quickly weakens as the mode number increases, in many cases it is sufficient to consider the second-mode instability only. For weakly coupled modes, the local dispersion relation is expressed in a simple analytical form that allows us to explain the intricate branching patterns observed in numerical solutions. These patterns depend on the locations of branch points in the complex plane (α plane for the temporal problem or R plane for the spatial stability problem describing propagation of disturbances in a weakly nonparallel boundary layer). Infinitesimal variations of a basic flow parameter (say, Mach number) can cause a jump from one branching pattern to another. Furthermore, in the branch-point vicinity, the modes are singular, e.g., their group velocities tend to infinity. Such unphysical behaviors indicate that instead of isolated normal modes one should consider an initial-boundary-value problem formulated for a certain physical setup.

To avoid confusion in terminology we recommend that authors use the terms fast modes (modes F_- and F_+) and slow mode (mode S) for both mathematical analyses and the interpretation of direct numerical simulations dealing with initial-value problems. For interpretation of experimental data and linear stability theory results focused on the characteristics of unstable disturbances, it is reasonable to continue to use Mack's terminology with the terms Mack's first mode and Mack's second mode. If both terminologies are involved, the correspondence between fast (or slow) modes and Mack's first (or second) modes should be established.

The aforementioned singularities of the discrete spectrum may cause difficulties in stability analyses based on traditional linear stability theory and parabolized stability equation methods. Multiple-mode considerations are needed to clarify this issue. This could be done using approximate theoretical models or by solving the linearized Navier–Stokes equations. Direct numerical simulations are also needed to validate predictions of the reduced-order models.

Acknowledgments

This work was sponsored by the U.S. Air Force Office of Scientific Research (AFOSR), National Center for Hypersonic Research in Laminar-Turbulent Transition (A. F. and A. T.), and by AFOSR, grant no. FA9550-08-1-0322 (A.T.) monitored by J. D. Schmisseur. The views and conclusions contained herein are those of the authors and should not be interpreted as representing the official polices or endorsements, either expressed or implied, of the AFOSR or the U.S. Government.

References

[1] Criminale, W. O., Jackson, T. L., and Joslin, R. D., *Theory and Computation in Hydrodynamic Stability*, Cambridge Univ. Press, New York, 2003.

[2] Mikhailovskii, A. B., *Theory of plasma instabilities*, Vol. 2, 1974, pp. 60–62.

[3] Gustavsson, L. H., "Initial-Value Problem for Boundary Layer Flows," *Physic of Fluids*, Vol. 22, 1979, pp. 1602–1605. doi:10.1063/1.862819

[4] Salwen, H., and Grosch, C. E., "The Continuous Spectrum of the Orr-Sommerfeld Equation. Part 2. Eigenfunction Expansion," *Journal of Fluid Mechanics*, Vol. 104, 1981, pp. 445–465. doi:10.1017/S0022112081002991

[5] Ashpis, D., and Reshotko, E., "The Vibrating Ribbon Problem Revisited," *Journal of Fluid Mechanics*, Vol. 213, 1990, pp. 531–547. doi:10.1017/S0022112090002439

[6] Tumin, A. M., and Fedorov, A. V., "Spatial Growth of Disturbances in a Compressible Boundary Layer," *Journal of Applied Mechanics and Technical Physics*, Vol. 24, 1984, pp. 548–554. doi:10.1007/BF00907906

[7] Balakumar, P., and Malik, M. R., "Discrete Modes and Continuous Spectra in a Mach 2 Boundary Layer," *Instability, Transition and Turbulence*, edited by M. Y. Hussaini, A. Kumar, and C. L. Streett, Springer–-Verlag, Berlin, 1992, pp. 242–252.

[8] Mack, L. M., "Boundary Layer Stability Theory," JPL Rept. 900-277. Jet Propulsion Lab., California Inst. of Technology, Pasadena, CA, May 1969.

[9] Fedorov, A. V., "Receptivity of a High-Speed Boundary Layer to Acoustic Disturbances," *Journal of Fluid Mechanics*, Vol. 491, 2003, pp. 101–129. doi:10.1017/S0022112003005263

[10] Tumin, A., "Biorthogonal Eigenfunction System in the Triple-Deck Limit," *Studies in Applied Mathematics*, Vol. 117, 2006, pp. 165–190. doi:10.1111/j.1467-9590.2006.00351.x

[11] Fedorov, A. V., and Khokhlov, A. P., "Prehistory of Instability in a Hypersonic Boundary Layer," *Theoretical and Computational Fluid Dynamics*, Vol. 14, 2001, pp. 359–375. doi:10.1007/s001620100038

[12] Guschin, V. R., and Fedorov, A. V., "Qualitative Properties of the Instability of Currents at a Wall in the Presence of a Flow at High Supersonic Speeds," NASA TT-20683, April 1990.

[13] Guschin, V. R., and Fedorov, A. V., "Excitation and Development of Unstable Disturbances in Supersonic Boundary Layer," *Fluid Dynamics*, Vol. 25, No. 3, 1990, pp. 344–352. doi:10.1007/BF01049814.

[14] Fedorov, A. V., "Transition and Stability of High-Speed Boundary Layers," *Annual Review of Fluid Mechanics*, Vol. 43, 2011, pp. 79–95. doi:10.1146/annurev-fluid-122109-160750

[15] Egorov, I. V., Fedorov, A. V., and Soudakov, V. G., "Numerical Modeling of the Receptivity of a Supersonic Boundary Layer to Acoustic Disturbances," *Fluid Dynamics*, Vol. 41, No. 1, 2006, pp. 37–48. doi:10.1007/s10697-006-0020-4

[16] Tumin, A., Wang, X., and Zhong, X., "Direct Numerical Simulation and the Theory of Receptivity in a Hypersonic Boundary Layer," *Physics of Fluids*, Vol. 19, 2007, Paper 014101. doi:10.1063/1.2409731

[17] Wang, X., and Zhong, X., "Role of the Synchronization Point on Boundary Layer Stabilization Using Porous Coating," AIAA Paper 2008-4382, Seattle, WA, 23–26 June 2008.

[18] Egorov, I. V., Fedorov, A. V., and Soudakov, V. G., "Receptivity of a Hypersonic Boundary Layer over a Flat Plate with a Porous Coating," *Journal of Fluid Mechanics*, Vol. 601, 2008, pp. 165–187.

[19] Fedorov, A., and Tumin, A., "Initial-Value Problem for Hypersonic Boundary Layer Flows," *AIAA Journal*, Vol. 41, 2003, pp. 379–389. doi:10.2514/2.1988

[20] Forgoston, E., and Tumin, A., "Initial-Value Problem for Three-Dimensional Disturbances in a Hypersonic Boundary Layer," *Physics of Fluids*, Vol. 17, 2005, Paper 084106. doi:10.1063/1.2013261

[21] Fedorchenko, A. M., and Kotsarenko, N. I., *Absolute and Convective Instabilities in Plasmas and Solids*, Nauka, Moscow, 1981 (in Russian).

[22] Lifshitz, E. M., and Pitaevskii, L. P., *Fizicheskaya Kinetika*, Nauka, Moscow, 1979; also "Physical Kinetics," *Course of Theoretical Physics*, Vol. 10, edited by L. D. Landau, and E. M. Lifshitz, Pergamon, Oxford, 1981 (in English).

[23] Guschin, V. R., and Fedorov, A. V., "Short-Wave Instability in a Perfect-Gas Shock Layer," *Fluid Dynamics*, Vol. 24, No. 1, 1989, pp. 7–10. doi:10.1007/BF01051470

[24] Ma, Y. B., and Zhong, X. L., "Receptivity of a Supersonic Boundary Layer over a Flat Plate. Part 1. Wave Structures and Interactions," *Journal of Fluid Mechanics*, Vol. 488, 2003, pp. 31–78. doi:10.1017/S0022112003004786

[25] Ma, Y. B., and Zhong, X. L., "Receptivity of a Supersonic Boundary Layer over a Flat Plate. Part 2. Receptivity to Free-Stream Sound," *Journal of Fluid Mechanics*, Vol. 488, 2003, pp. 79–121. doi:10.1017/S0022112003004798

X. Zhong
Associate Editor